Clim Dyn (2014) 42:1243–1258
DOI 10.1007/s00382-013-1721-0

Interannual and interdecadal variability of ocean temperature along the equatorial Pacific in conjunction with ENSO

Arun Kumar · Zeng-Zhen Hu

Received: 16 October 2012 / Accepted: 4 March 2013 / Published online: 19 March 2013

Abstract In this paper, the leading modes of ocean temperature anomalies (OTA) along the equatorial Pacific Ocean are analyzed and their connection with El Niño-Southern Oscillation (ENSO) and interdecadal variation is investigated. The first two leading modes of OTA are connected with the different phases of the canonical ENSO and display asymmetric features of ENSO evolution. The third leading mode depicts a tripole pattern with opposite variation of OTA above the thermocline in the central Pacific to that along the thermocline in the eastern and western Pacific. This mode is found to be associated with so-called ENSO-Modoki. Insignificant correlations of this mode with the first two leading modes suggest that ENSO-Modoki may be a mode that is independent to the canonical ENSO and also has longer time scales compared with the canonical ENSO. The fourth mode reflects a warming (cooling) tendency above (below) the thermocline since 2000. Both the first and second modes have a large contribution to the interdecadal change in thermocline during 1979–2012. Also, the analysis also documents that both ENSO and OTA shifted into higher frequency since 2000 compared with that during 1979–1999. Interestingly, the ENSO-Modoki related OTA mode does not have any trend or significant interdecadal shift during 1979–2012. In addition, it is shown that first four EOF modes seem robust before and after 1999/2000, suggesting that the interdecadal shift of the climate system in the tropical Pacific is mainly a frequency shift and the changes in spatial pattern are relatively small, although the mean states over two periods experienced some significant changes.

A. Kumar · Z.-Z. Hu (✉)
Climate Prediction Center, NCEP/NWS/NOAA, 5830 University Research Court, College Park, MD 20740, USA
e-mail: zeng-zhen.hu@noaa.gov

Keywords ENSO · Ocean temperature along the equatorial pacific · Tilt mode · Warm water volume mode · ENSO-Modoki · Interannual and interdecadal variations

1 Introduction

El Niño–Southern Oscillation (ENSO) is the leading mode of interannual variability in the tropical climate system having significant impact on global weather and climate anomalies (e.g., Ropelewski and Halpert 1987; Glantz 2000). ENSO is also the primary source for making skillful seasonal and interannual climate predictions (Kumar et al. 2005; National Research Council 2010). As a consequence, understanding of the physics behind ENSO variability and improving its prediction have been a major area of research in the last few decades (Guilyardi et al. 2009; National Research Council 2010).

Physically, ENSO is a manifestation of coupled air-sea interactions in the tropical Pacific Ocean (Bjerknes 1969; Barnett et al. 1991; Neelin et al. 1998; Wang and Picaut 2004; Guilyardi et al. 2009). Climatologically, warm water in the west and cold water in the east represents an equilibrium between prevailing easterly winds and the tilt of the thermocline along the equatorial Pacific. Bjerknes (1969) proposed that a region of anomalously warm anomaly in the tropical eastern Pacific can weaken the east–west sea surface temperatures (SST) gradient, leading to a relaxation of the trade winds that are a part of the Walker circulation in the equatorial Pacific. As a consequence, equatorial upwelling, which normally brings colder water from the subsurface to the surface and causes surface cooling in the eastern Pacific also diminishes due to the weakening of the trade winds. In the Bjerknes (1969) proposed mechanism, the subsurface change connected with thermocline slope variation is largely

a balance adjustment to changes in the surface trades. Warming of SST in the eastern Pacific reduces the west-to-east SST gradient, thus further weakening trade winds, that in turn, amplify the warming in the tropical eastern Pacific. This positive feedback between the trade winds and SST zonal gradient results in relatively long-lasting atmospheric and oceanic anomalies with large amplitude in the tropical Pacific, and are collectively referred to as ENSO.

ENSO, however, is not only associated with changes of surface trade wind and SST, but is also manifested as changes in the sub-surface ocean variability (e.g., Zhang and Levitus 1996; Meinen and McPhaden 2000; Clarke 2010). Indeed, sub-surface changes in the ocean provide the memory and mechanism for the ENSO turnaround from one phase to another, e.g., from El Niño to La Niña or vice versa, that originally was absent in the Bjerknes mechanism. Sub-surface changes in the ocean are a response to changes in surface winds leading to a displacement (or perturbation) in the climatological thermocline. Thus, the ENSO cycle is actually an interaction between the trade wind, the zonal SST gradient along the equatorial Pacific, and the thermocline (e.g., Zhang and Levitus 1997; Meinen and McPhaden 2000; An and Jin 2001; Clarke et al. 2007). Although the surface characteristics of ENSO have been studied extensively, the thermocline variation and its relation with ENSO have been examined less systematically due to shortage of the sub-surface observational data (Zhang and Levitus 1996, 1997; Meinen and McPhaden 2000; Moon et al. 2004; Clarke et al. 2007; Clarke 2010; Dewitte et al. 2009; Yu et al. 2011).

Previous investigations have demonstrated that ENSO associated with ocean temperature anomalies (OTA) along the equatorial Pacific is mainly manifested as two leading patterns of variability. One is with an opposite variation along the thermocline between the western and eastern Pacific (Zhang and Levitus 1996, 1997; Jin 1997a, b), and is generally referred as tilt mode (Meinen and McPhaden 2000; Clarke et al. 2007; Clarke 2010). It has been suggested that this mode is mainly driven by zonal wind stress (Clarke et al. 2007; Clarke 2010). The other mode is associated with variations in warm water volume (WWV). It is called WWV mode and driven by surface wind stress curl meridional gradient (Meinen and McPhaden 2000; Clarke et al. 2007; Clarke 2010). In fact, time evolution of the tilt mode and WWV mode is in quadrature, leading to the oscillatory feature of ENSO.

Recently considerable focus has been given to "different flavors of ENSO" (Weare et al. 1976; Hoerling and Kumar 2002; Trenberth and Smith 2006). For example, besides the canonical ENSO, ENSO-Modoki (Ashok et al. 2007), also referred to as warm pool El Niño (Kug et al. 2009; Hu et al. 2012), or central Pacific El Niño (Kao and Yu 2009), were emphasized in recent years. Although having similarities, the canonical ENSO and ENSO-Modoki also have distinguishing features in their spatial pattern, and life cycle, as well as their associated physical processes. For example, the canonical ENSO (ENSO-Modoki) is associated with stronger (weaker) and more eastward extended (westward confined) westerly wind along the equatorial Pacific in the early months of a year preceding the event development, as well as more (less) well defined oceanic thermocline feedback (Hu et al. 2012). However, it is unclear what are the difference and connection of the OTA distribution associated with the canonical ENSO and ENSO-Modoki. Moreover, it is unclear whether the difference of OTA between canonical ENSO and ENSO-Modoki is more likely due to lack of cold tongue weakening in the former, although it seems that eastward expansion of the warm pool is a universal feature shared by both canonical ENSO and ENSO-Modoki (e.g., Picaut et al. 1996; Kao and Yu 2009; Kug et al. 2009, 2010; Hu et al. 2012).

The connection of ENSO with the OTA may also be modulated by interdecadal variation in the coupled system in the tropical Pacific. Recently, McPhaden (2012) documented a shift of the relationship between ENSO and WWV integrated along the equatorial Pacific around 1999/2000. He reported that while WWV led ENSO SST anomalies by 2–3 seasons during the 1980/1990s, variability in WWV decreased and lead time was reduced to only one season during the 2000s. Horii et al. (2012) also argued that compared with 1981–2000, the interrelationship of the WWV and ENSO weakened after 2000, especially for El Niño/La Niña events in 2005–2011. Hu et al. (2013a) documented a coherent weakening of the interannual variability of the ocean–atmosphere system in the tropical Pacific in 2000–2011, compared with 1979–1999. For example, the equatorial thermocline tilt became steeper during 2000–2011, and was consistent with positive (negative) sea surface temperature anomalies, increased (decreased) precipitation, and enhanced (suppressed) convection in the western (central and eastern) tropical Pacific, which reflected an intensification of the Walker circulation. Both McPhaden (2012) and Horii et al. (2012) speculated that the change of the relationship between WWV and ENSO may be linked to a shift towards more central Pacific versus eastern Pacific El Niños in the past decade. Hu et al. (2013a) argued that the combination of a steeper thermocline slope with stronger surface trade winds hampers the eastward migration of the warm water along the equatorial Pacific. As a consequence, the variability of the warm water volume was reduced, and thus, ENSO amplitude also decreased. Thus, it is an interesting topic to further examine the connection of the variability of OTA with different flavors of ENSO and their interdecadal variations.

In this work, we focus on the leading modes of variability in OTA along the equatorial Pacific in context with

ENSO and ENSO-Modoki evolution. First, the spatial patterns and temporal behaviors of the major modes of OTA variability are examined with the method of empirical orthogonal function (EOF) analysis. Then, the connections of these modes with the ENSO cycle and ENSO-Modoki, as well as interdecadal variations are investigated. The paper is organized as following. After the introduction section, the data used in this work are briefly introduced in Sect. 2. In Sect. 3, we present the results, followed by a summary and discussion in Sect. 4.

2 Data

A main dataset used in this work is from the global ocean data assimilation system (GODAS) (Behringer and Xue 2004). The ocean model in GODAS is based on the Geophysical Fluid Dynamics Laboratory Modular Ocean Model version 3 in a quasi-global (75°S–65°N) configuration with climatological sea-ice. The spatial resolution is 1° in zonal direction and 1/3° in meridional direction between 10°S and 10°N, gradually increasing through the tropics to 1° poleward of 30°S and 30°N. There are 40 vertical layers with 27 layers in the upper 400 meter (m) of the oceans.

GODAS is forced with the atmospheric fluxes from the National Centers for Environmental Prediction/Department of Energy (DOE) reanalysis (Kanamitsu et al. 2002). In each assimilation cycle, the model state is corrected by observations within a 4 week window centered on the assimilation time using a three-dimensional variational data assimilation scheme. The assimilated observational data include temperature profiles from expendable bathythermographs, tropical atmosphere ocean (TAO), Triangle Trans Ocean Buoy Network, Pilot Research Moored Array, and Argo profiling floats. Only the temperature data in the top 750 m are assimilated into GODAS. Due to the lack of direct salinity observations, synthetic salinity profiles constructed from temperature and a local temperature-salinity climatological relationship are also assimilated. More details about the data assimilation system can be found in Behringer and Xue (2004) and Huang et al. (2010).

In addition to the direct use of ocean temperature, WWV is also used in the analysis, which is defined as average depth of 20 °C (d20) over (120°E–80°W, 5°S–5°N) (Meinen and McPhaden 2000) and is calculated using GODAS data. The variability of WWV measures the recharge and discharge processes involved in ENSO (Jin 1997a, b; Meinen and McPhaden 2000). Monthly mean ocean temperature, and WWV data span the period Jan 1979–Dec 2012.

To verify the GODAS data, we also use TAO ocean temperature profiles between the ocean surface and 500 m along the equatorial Pacific, which are the objective equatorial TAO temperature analysis averaged between 2°S and 2°N in the period Jan 1993–Dec 2012 (McPhaden 1993). Based on the comparison of the mean state and variance (not shown), we conclude that ocean temperature in the top 500 m along the equatorial Pacific is almost identical between GODAS and TAO, confirming the reliability of GODAS data.

In addition to the monthly mean SST data, Niño3.4 and ENSO-Modoki indices are computed using version 3b of the extended reconstruction of the SST analyses (ERSSTv3) on a $2^\circ \times 2^\circ$ grid during the period Jan 1979–Dec 2012 (Smith et al. 2008). Niño3.4 is the average SST anomaly in the region (5°N–5°S, 170°W–120°W). Following Ashok et al. (2007), to capture the tripolar nature of SST anomalies (SSTA) associated with ENSO-Modoki, an ENSO-Modoki index is defined as $\left\{ [\overline{\text{SSTA}}]_{(165^\circ\text{W}-140^\circ\text{W},\, 10^\circ\text{S}-10^\circ\text{N})} - 1/2 \; [\overline{\text{SSTA}}]_{(110^\circ\text{W}-70^\circ\text{W},\, 15^\circ\text{S}-5^\circ\text{N})} - 1/2 \; [\overline{\text{SSTA}}]_{(125^\circ\text{E}-145^\circ\text{E},\, 10^\circ\text{S}-20^\circ\text{N})} \right\}$. All the anomalies are with respect to the climatology computed over their respective period for each calculation.

3 Results

We first show the leading modes of EOF of OTA in GODAS and TAO data and then investigate their connection with the canonical ENSO and ENSO-Modoki by examining lead-lag correlation with Niño3.4, ENSO-Modoki, and WWV indices. EOF is computed using ocean temperature anomalies (OTA) along the equatorial Pacific averaged between 2°S and 2°N in 0–459 m for GODAS (28 levels) during Jan 1979–Dec 2012 and in 0–500 m for TAO (24 levels) during Jan 1993–Dec 2012. The layer of 459 m is the closest layer to 500 m in GODAS, the next layer is 585 m. EOF was calculated using covariance matrix with square root of vertical thickness of each layer represented as weight. Lastly, we compare the contribution of each mode to the interdecadal variations through EOF reconstruction. In the following, we note that between GODAS and TAO the first four leading modes of OTA show an almost identical spatial pattern and temporal evolution over the common period, and similar variances explained by each mode. Although it could be argued that this may be because of TAO data being assimilated in GODAS, it gives us the confidence in using relatively longer GODAS OTA data to examine its connection with the canonical ENSO and ENSO-Modoki as well as the interdecadal shift.

3.1 Tilt mode and ENSO

Figure 1 depicts EOF1 and PC1 of OTA of GODAS and TAO, which explain 49 and 56 % of their corresponding total variances, respectively. EOF1 is characterized by opposite variation of OTA between the eastern (cold tongue region) and western (warm pool region) equatorial Pacific (Fig. 1c, d). This mode bears some similarities with EOF1 of yearly mean OTA along the equator shown in Zhang and Levitus (1997) (see their Fig. 14a) and it is also similar to the OTA distribution pattern during the ENSO mature phase shown in Meinen and McPhaden (2000), Kug et al. (2009), Kao and Yu (2009), Hu et al. (2012), and represents a change in the east–west tilt of the thermocline associated with ENSO variability. This mode is generally referred to as the tilt mode (Clarke 2010). We note that the positive loading center in the east is almost along the thermocline and the negative one in the west is slightly above the mean thermocline. Also, the magnitude of anomaly is larger for the positive center than for the negative center (Fig. 1c, d), highlighting the asymmetric amplitude of the OTA in the eastern and western equatorial Pacific associated with ENSO. This asymmetry is likely related to the mean depth of the thermocline that being shallower in the east is more susceptible to surface wind variations related to ENSO, and as a consequence, has stronger thermocline feedback (An and Jin 2001).

For PC1, its positive excursions are larger than their negative counterpart (shading of Fig. 1a, b), consistent with the asymmetry of SSTA between El Niño and La Niña. Statistically, SSTA over the equatorial Pacific cold tongue have larger magnitude during El Niño compared to that

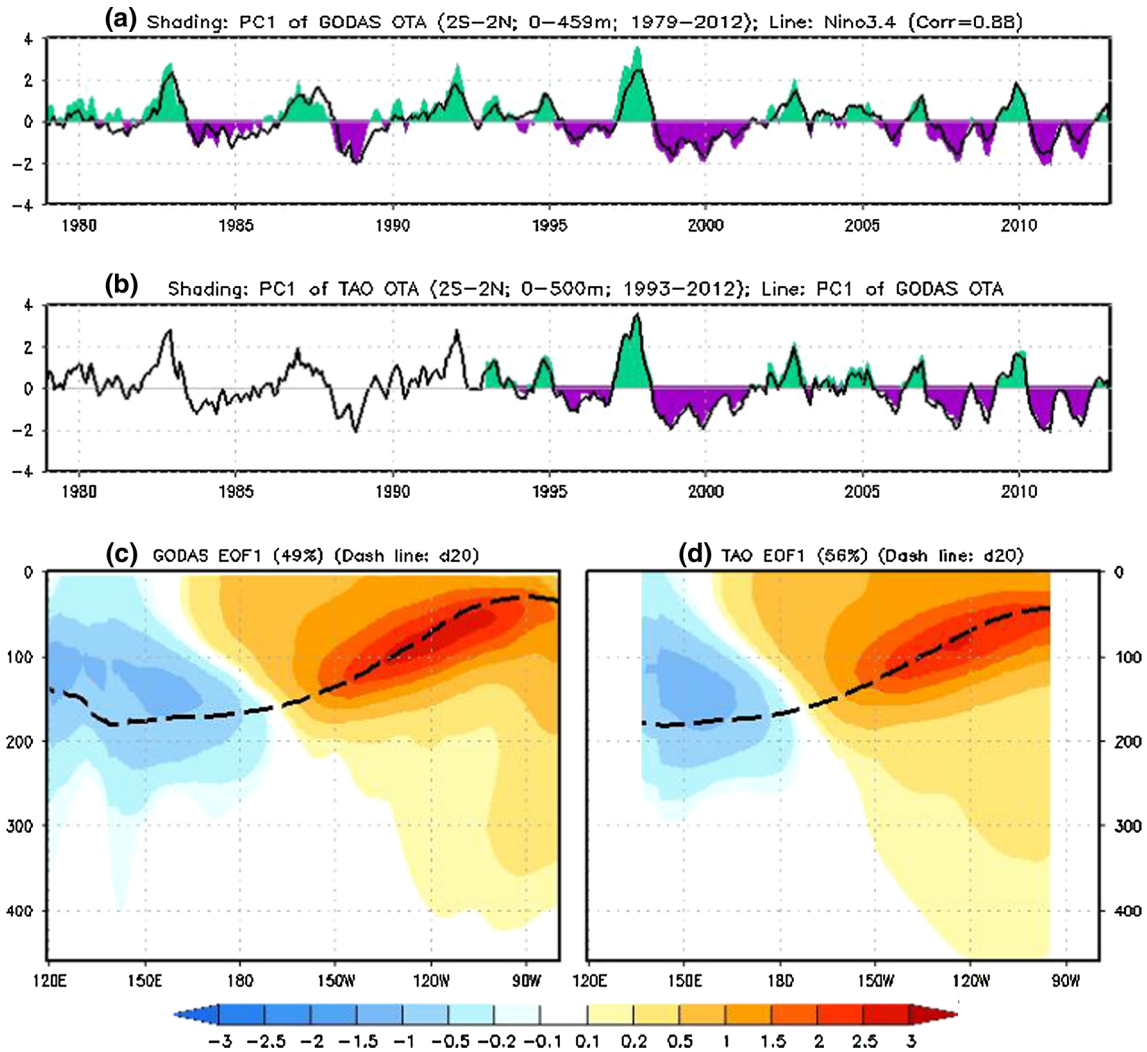

Fig. 1 (**a**) PC1 of GODAS (*shading*) and Niño3.4 index (*curve*); (**b**) PC1 of TAO (*shading*) and PC1 of GODAS (*curve*); (**c**) EOF1 of GODAS; and (**d**) EOF1 of TAO. The percentage of total variance explained by this mode is 49 % for GODAS and 57 % for TAO, respectively. The spatial loading pattern is shown only between the surface and 459 m and the *dash line* in (**c**, **d**) is the climatological mean depth of 20 °C (d20)

during La Niña resulting in positive skewness of interannual SST variations (Burgers and Stephenson 1999; Okumura and Deser 2010). Burgers and Stephenson (1999) argued that largest SST skewness observed in the eastern equatorial Pacific is due to the fact that as the thermocline is already close to the surface, departures on the cold side are constrained by the temperature below the thermocline reaching the surface. The negative skewness in the warm pool region is most likely caused by SSTs saturating at 30 °C due to radiative convective equilibrium and feedbacks.

PC1 temporal evolution associated with El Niño and La Niña events is also not symmetric. On average, PC1 returns to zero faster after the mature phase of El Niño than that for La Niña (shading of Fig. 1a, b). This feature is consistent with the evidence that after the mature phase El Niño tends to decay rapidly by next summer, but many La Niñas persist through the following year and often re-intensify in the subsequent winter (Kessler 2002; Okumura and Deser 2010; Hu et al. 2013b). Okumura et al. (2011) argued that the eastward displacement of atmospheric deep convection anomalies during El Niño enables surface winds in the western equatorial Pacific to be more affected by remote forcing from the Indian Ocean, leading to a faster termination of warm ENSO events in the Pacific. Recently, Hu et al. (2013b) argued that a precondition of La Niña occurrence in consecutive years is that it must be a strong event (i.e., a major La Niña), ensuring that reflected Rossby wave signals at the eastern boundary of the Pacific have strong westward propagating cold anomaly over the off-equatorial region. The off-equator cold anomaly is not conducive to the recharge process, and as a result, favors the persistence of anomalously cold ocean subsurface and preventing transition to El Niño.

The connection of EOF1 of the OTA with the ENSO cycle is further examined by computing lead and lag correlations between PC1 (based on GODAS) and Niño3.4

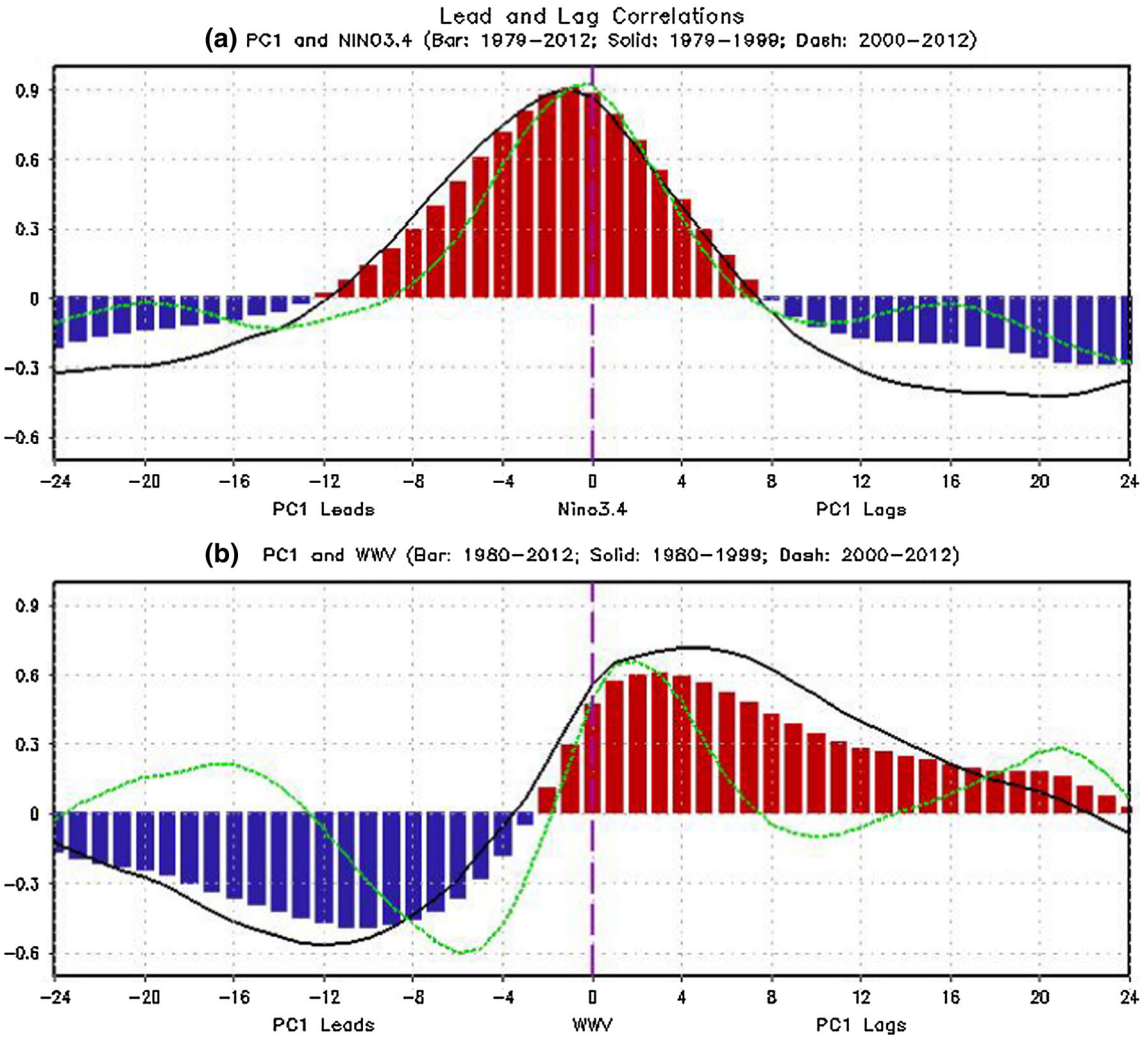

Fig. 2 Lead and lag correlations between (**a**) PC1 and Niño3.4 index (**b**) PC1 and warm water volume (WWV) index. *Bar* is the correlations for the whole period, *solid line* for Jan 1979/1980–Dec 1999, and *dash line* for Jan 2000–Dec 2012

index (bars in Fig. 2a). The simultaneous correlation between PC1 and Niño3.4 index is 0.88 (Fig. 1a), confirming the strong in-phase relationship in the variations of the east–west gradient in the thermocline with ENSO (as captured by the Niño3.4 index) (Philander 1990; Neelin et al. 1998; Meinen and McPhaden 2000; Wang and Picaut 2004). The strongest correlation occurs when PC1 leads the Niño3.4 index by 0–2 months, indicating EOF1 subsurface OTA pattern leading the ENSO peak by a couple months. The leading in the evolution of OTA, and its emergence as variations in the Niño3.4 SST, may be related to a time scale that is associated with the establishment of the air-sea coupling after sub-surface temperature anomalies emerge at the surface and intensify further through Bjerknes feedback (Bjerknes 1969).

WWV variability in the equatorial Pacific has also been linked with the ENSO variability (Meinen and McPhaden 2000), and therefore, the connection between EOFs of OTA and WWV variability is also analyzed. As a reminder, WWV is the mean of depth of d20 averaged over (120°E–80°W, 5°S–5°N). The lead-lag correlation between WWV and PC1 of OTA (bars in Fig. 2b) shows considerable asymmetry in the sign of correlation. For example, when PC1 lags (leads), its correlation with WWV is positive (negative). It is well known that El Niño (La Niña) events are associated with discharge (recharge) of WWV subsequent to their peak phase (Jin 1997a, b; Meinen and McPhaden 2000) and this is reflected as a negative correlation when PC1 leads WWV. On the other hand, it is positive (negative) WWV anomalies that lead the onset of El Niño (La Niña) and this is reflected as positive correlation when PC1 lags WWV.

The relationships of PC1 with Niño3.4 and WWV experienced interdecadal changes. This is confirmed when the lead-lag correlations are computed over two periods separately: 1979–1999 and 2000–2012. It should be indicated that splitting the two periods from slightly different years does not affect results. Although the amplitudes of the correlations of PC1 with Niño3.4 and WWV for short lead and lag times are comparable for 2000–2012 (dashed line in Fig. 2a, b) and 1979–1999 (solid line in Fig. 2a, b), the differences of the correlations become pronounced with the increase of lead or lag times. We note that the differences of the correlations mainly reflect a change in the interannual variability instead of long-term change in the mean, since the correlations in the two periods are calculated with the climatology in each data period. The pronounced difference is mainly associated with a frequency change. For instance, the change of the correlation between PC1 and WWV suggests that frequency of subsurface ocean temperature variability became higher since 2000 than during 1979–1999 (solid and dashed lines in Fig. 2b). A similar change is also discernible in the autocorrelation for PC1 time series in that it has a faster decay since 2000 than before (Fig. 3a), and is indicative of higher frequency ENSO variability since 2000. This is consistent with McPhaden (2012) who reported that the WWV led ENSO SST anomalies by 2–3 seasons during the 1980/1990s, and the lead time was reduced to only one season during the 2000s. These features may imply that the coupled system in the tropical Pacific may have shifted to a different regime since 2000 (McPhaden 2012; Horii et al. 2012; Hu et al. 2013a). Also, these changes coincide with decreased prediction skill of ENSO events since 2000 compared with that during 1981–1999 (see Fig. 5b of Wang et al. 2010).

3.2 WWV mode and ENSO

EOF2 and PC2 of OTA of GODAS and TAO are shown in Fig. 4, and explain 25 and 24 % of their corresponding total variances for GODAS and TAO data, respectively. The spatial pattern of EOF2 (Fig. 4c, d) depicts an opposite variation between the central and eastern Pacific, and between 0 and 250 m and 250–650 m in the eastern Pacific. The structure of this mode is similar to the basin wide variations in d20 identified by Meinen and McPhaden (2000), and can be linked with the recharge-discharge paradigm of ENSO variability and turnaround of ENSO from one phase to its opposite phase, called WWV mode (Meinen and McPhaden 2000; Clarke 2010). Similar to PC1 (Fig. 1), the magnitude of positive phase of PC2 is also larger than its negative phase (Fig. 4a, b). We note that PC2 is dominated by 4–5 year and larger variations before 2000, and further, by higher frequency variation with smaller amplitude since 2000 (Fig. 4a).

The simultaneous correlation between GODAS PC2 and Niño3.4 index is much smaller with value of 0.24 (Fig. 4a), compared to that between PC1 and Niño3.4 index with value of 0.88 (Fig. 1a). In fact, the maximum positive correlation occurs when Niño3.4 index leads PC2 by 5–7 months (bars in Fig. 5a). This is because the peak phase of El Niño (La Niña) is followed by a discharge (recharge) of heat content (or WWV) in the equatorial Pacific. We note that the magnitude of maximum negative correlations between PC2 and WWV (bars in Fig. 5b) is greater than that of either positive or negative correlations between PC1 and WWV (bars in Fig. 3b), indicating a closer connection of PC2 with recharge-discharge processes. This is also reflected in lead-lag correlation between PC2 and WWV (bars in Fig. 5b). When PC2 is in its positive (negative) phase, corresponding to negative (positive) OTA in the subsurface extending over the equatorial Pacific (see Fig. 4c, d), WWV is negative (positive). This relationship was also noted by Meinen and McPhaden (2000) who found that the PC2 of the d20 has a very good correspondence with the time evolution of WWV.

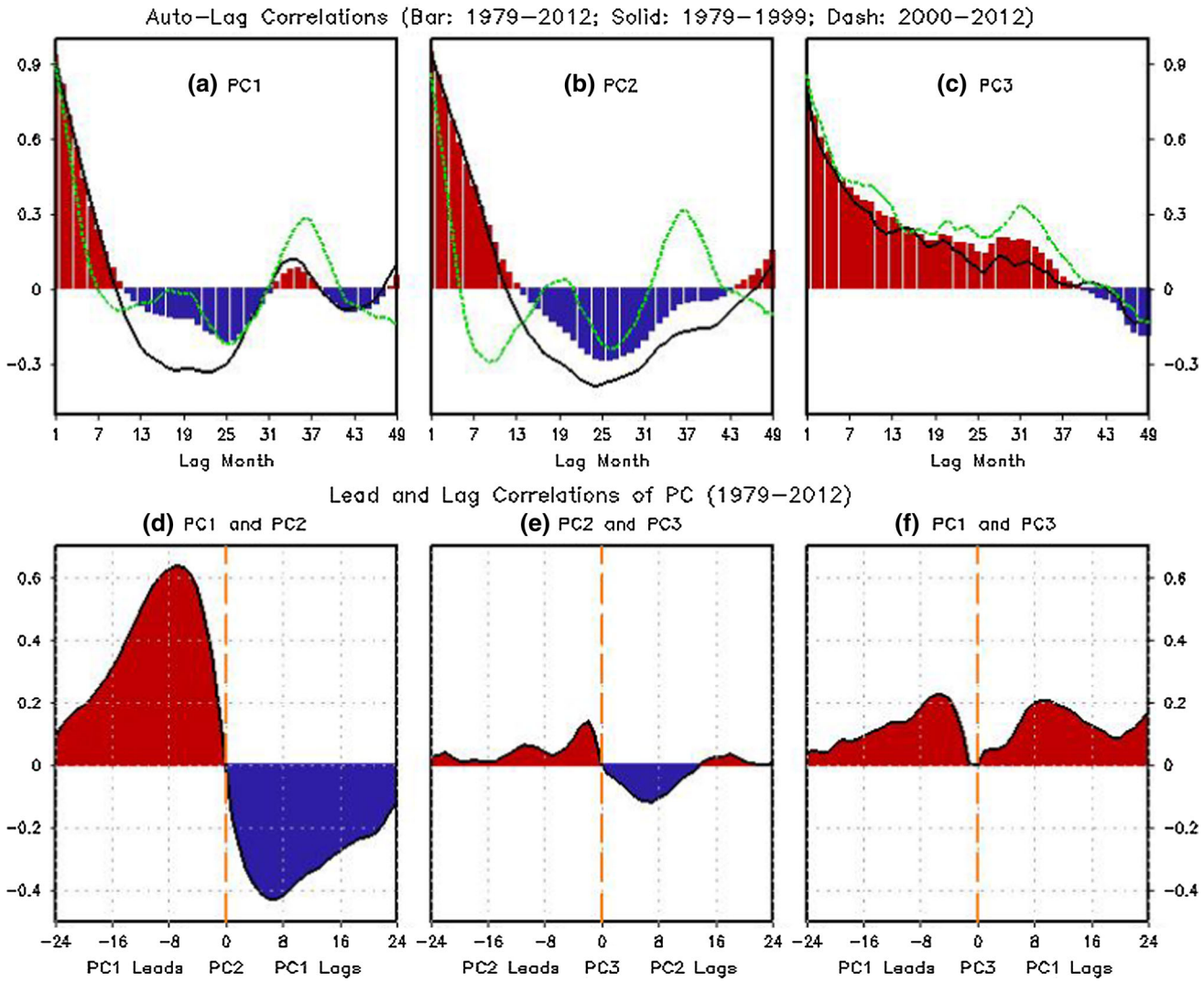

Fig. 3 Top panels: Auto-lag correlations of (**a**) PC1 (**b**) PC2 and (**c**) PC3. The *bar* is the correlations for the whole period, *solid line* for Jan 1979/1980–Dec 1999, and *dash line* for Jan 2000–Dec 2012. Bottom panels: lead and lag correlations between (**d**) PC1 and PC2 (**e**) PC2 and PC3, and (**f**) PC1 and PC3 in Jan 1979–Dec 2012

Similar to the interdecadal shift in the lead-lag correlation between PC1 and ENSO (Fig. 2), the connection between PC2 and ENSO (Fig. 5) also experienced a similar shift around 1999/2000, mainly for the frequency aspect of the variability. For instance, the correlation between PC2 and WWV consistently suggests that frequency of subsurface ocean temperature variability became higher since 2000 than during 1979–1999 (solid and dashed lines in Fig. 5b), and this fact is also evident from the autocorrelation for PC2 with faster decay in the autocorrelation since 2000 compared to the one before (Fig. 3b). A similar feature also presents in the correlations between PC2 and Niño3.4 index (solid and dashed lines in Fig. 5a).

With EOF1 as a proxy for ENSO (and east–west variations of the thermocline) and EOF2 as a proxy for WWV (with basin wide variations in the thermocline), the known relationships between WWV leading the ENSO events, and ENSO events (depending on their phase) leading to the recharge or discharge in the equatorial Pacific are brought out by lead-lag correlation between the time-series of PC1 and PC2 (Fig. 3d). With PC1 lagging PC2, the correlation is negative and peaks around 6–7 months, and is consistent with the buildup (decay) of ocean heat content leading to El Niño (La Niña) event. On the other hand, with PC1 leading PC2, a positive correlation that also peaks around 6–7 months is consistent with El Niño (La Niña) leading to a discharge (recharge) of ocean heat content in the equatorial Pacific. This is consistent with the quadrature relationship between the tilt and WWV modes indicated in Meinen and McPhaden (2000) and Clarke (2010).

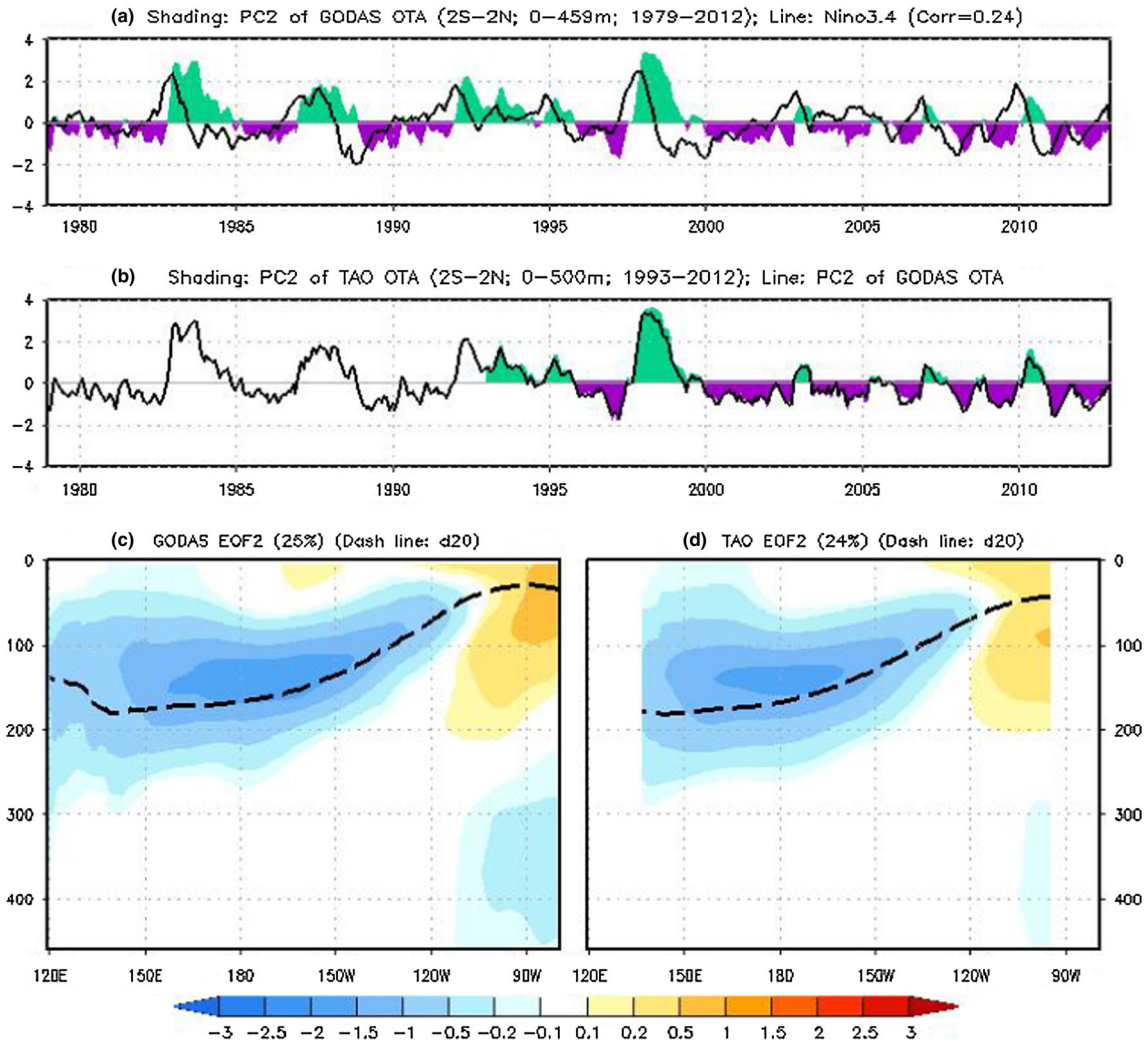

Fig. 4 Same as Fig. 1, but (**a**) PC2 of GODAS (*shading*) and Niño3.4 index (*curve*); (**b**) PC2 of TAO (*shading*) and PC2 of GODAS (*curve*); (**c**) EOF2 of GODAS; and (**d**) EOF2 of TAO. The percentage of total variance explained by this mode is 25 % for GODAS and 24 % for TAO, respectively

3.3 EOF3 and ENSO-Modoki

EOF3 shows a tripole pattern with opposite variation of OTA in the central Pacific with that in the eastern and western Pacific (Fig. 6c, d), and explains 7 and 6 % of their respective total variances for GODAS and TAO data, respectively. The sub-surface temperature anomaly in the central Pacific stays mainly above the mean thermocline, a feature also noted by Kim et al. (2012). This mode is tied up with the so-called ENSO-Modoki, warm pool ENSO, or the central Pacific ENSO. The simultaneous correlation between PC3 and ENSO-Modoki index (Ashok et al. 2007) is 0.61 (Fig. 6a), and the maximum positive correlation occurs when ENSO-Modoki index lags PC3 by 0–1 months (bars in Fig. 7a). Also, all the correlations are positive in the 24 month lead and lag window (bars in Fig. 7a) due to the low frequency variation feature of PC3 (Fig. 6a, b). This may imply a relatively longer period for ENSO-Modoki compared with the canonical El Niño. It is not clear why the time scales associated with this mode are longer than the first two modes. A possibility is that the El Niño Modoki events maybe relate to the variability in the North Pacific Oscillation (Vimont et al. 2009; Di Lorenzo et al. 2010; Kim et al. 2012).

The magnitudes of both positive and negative centers of EOF3 (Fig. 6c, d) are much smaller than for the corresponding EOF1 (Fig. 1c, d) and EOF2 (Fig. 4c, d). On the other hand, compared with EOF1 and EOF2 (Figs. 3b, 5b), the evolution of EOF3 is only weakly correlated with WWV with correlation coefficients between −0.2 and 0.2 (bars in Fig. 7b). The magnitudes of the lead and lag correlations between PC2 and PC3 (Fig. 3e) and between PC1 and PC3 (Fig. 3f) are <0.25. Collectively, the ENSO-Modoki mode does involve the thermocline processes, but

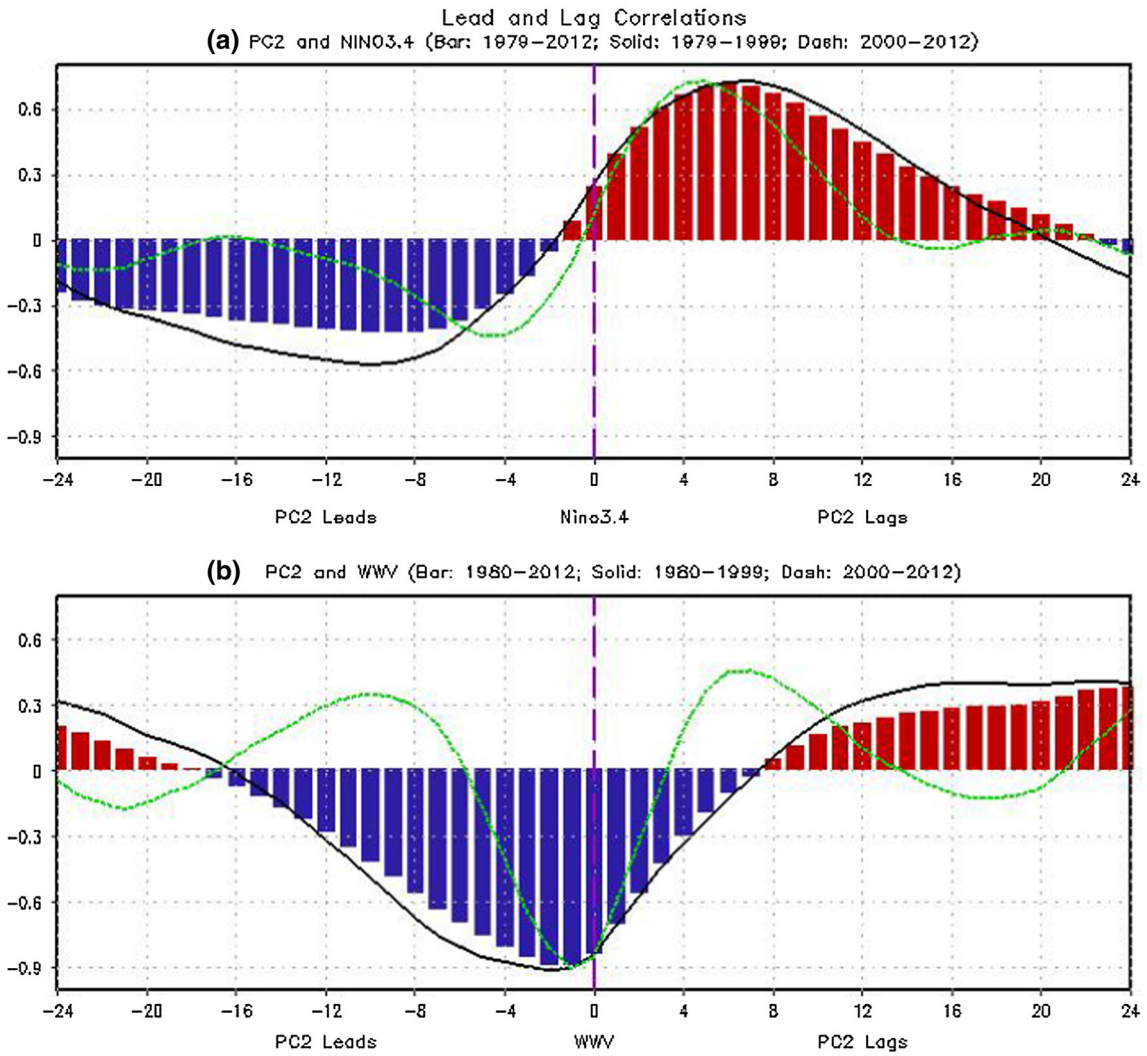

Fig. 5 Lead and lag correlations between (**a**) PC2 and Niño3.4 index (**b**) PC2 and WWV index. *Bar* is the correlations for the whole period, solid line for Jan 1979/1980–Dec 1999, and dash line for Jan 2000–Dec 2012

the associated anomalies are weaker and have a different pattern compared with that associated with the canonical ENSO. This agrees with previous investigations (e.g., Ashok et al. 2007; Kug et al. 2009; Kao and Yu 2009; Hu et al. 2012; Kim et al. 2012). They argued that ENSO-Modoki is a physical mode independent to the canonical ENSO and less actively involves thermocline processes compared with the canonical ENSO.

Importantly, the ENSO-Modoki mode does not show any trend in its temporal evolution during the data period (1979–2012) (Fig. 6a, b). This is consistent with L'Heureux et al. (2013) who argued that upward trend of ENSO-Modoki suggested in some previous works is not due to the change of the ENSO-Modoki mode itself, but is due to the mean state change, such as zonal SST gradient increase between Niño4 and Niño3 regions in the Northern Hemisphere spring (Mar–May) during both El Niño and La Niña and also in the late summer/early fall (Jul–Sep) during El Niño. Furthermore, there is no significant interdecadal change in correlations between PC3 and ENSO-Modoki index (Fig. 7a), as well as in its autocorrelation before and after 1999/2000 (Fig. 3c).

3.4 EOF4 and robustness of the first four leading modes

EOF4 explains a small fraction (3 %) of the total variance in OTA in the equatorial Pacific in both GODAS and TAO data, and is characterized by opposite variation between above and below the thermocline (Fig. 8c, d). Interestingly, PC4 is dominated by a sudden jump from a period dominated by negative to a period dominated by positive values around 1999/2000 (Fig. 8a, b). Thus, this mode reflects a tendency of warming above the thermocline and cooling

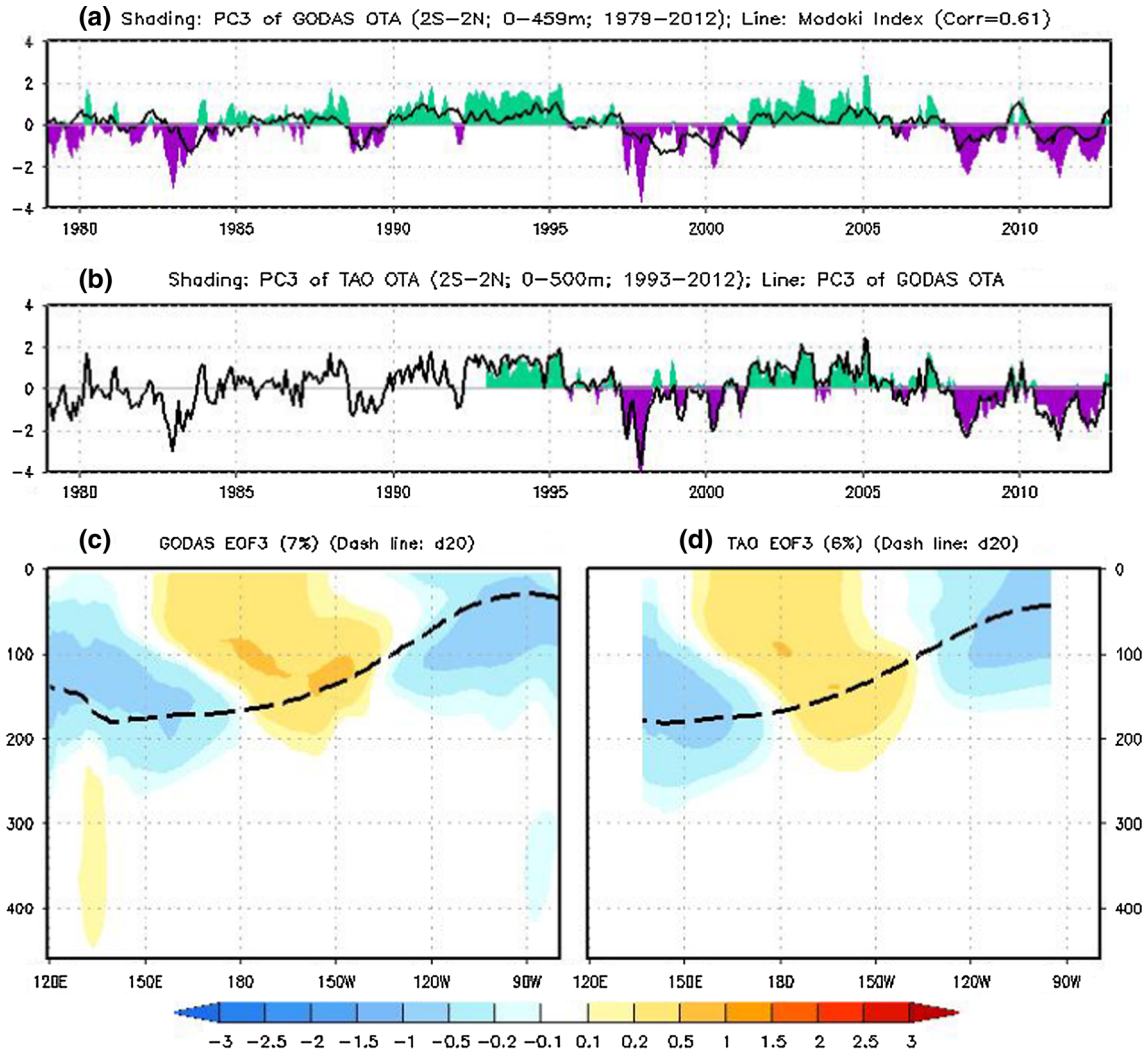

Fig. 6 Same as Fig. 1, but (**a**) PC3 of GODAS (*shading*) and ENSO Modoki index (*curve*); (**b**) PC3 of TAO (*shading*) and PC3 of GODAS (*curve*); (**c**) EOF3 of GODAS; and (**d**) EOF3 of TAO. The percentage of total variance explained by this mode is 6 % for both GODAS and TAO

below the thermocline since 2000. Recently, Kumar et al. (2012), L'Heureux et al. (2013) and Xue et al. (2013) argued that change in surface wind stress around 1999/2000 might be a factor resulting in the warming and cooling tendency mentioned here, albeit it needs to be further confirmed.

Interestingly, it is noted that this mode seems robust, although it explains small fraction of the total variance. For example, in a similar EOF analysis, but only using data in Jan 2000–Dec 2012, a similar mode does present as EOF4 (Fig. 9d). This may imply that there may be some physically realistic variabilities of OTA which do have projection onto this mode.

Furthermore, in addition to the robustness of EOF4, EOFs 1–3 are also robust. The spatial patterns of EOF 1–3 using data in Jan 2010–Dec 2012 (Fig. 9a, b, c) are analogues to that using data in Jan 1979–Dec 2012 (Figs. 1c, 4c, 6c, 8c), in spite of some detailed differences. That may suggest that the interdecadal shift of the climate system in the tropical Pacific is mainly a frequency shift (McPhaden 2012). Meanwhile, the spatial variation pattern changes are relatively small, although the mean states have experienced some significant changes (Hu et al. 2013a).

3.5 Changes in the thermocline and contribution from different EOFs

Recent literature documented an enhanced east–west tilt in the thermocline in the equatorial Pacific with the thermocline being deeper (shallower) in western (eastern) Pacific (Fig. 10a) since 2000 (Hu et al. 2013a). With the decomposition of sub-surface OTA variability into different modes, we investigate which modes might have contributed to the changes in the thermocline. This is achieved

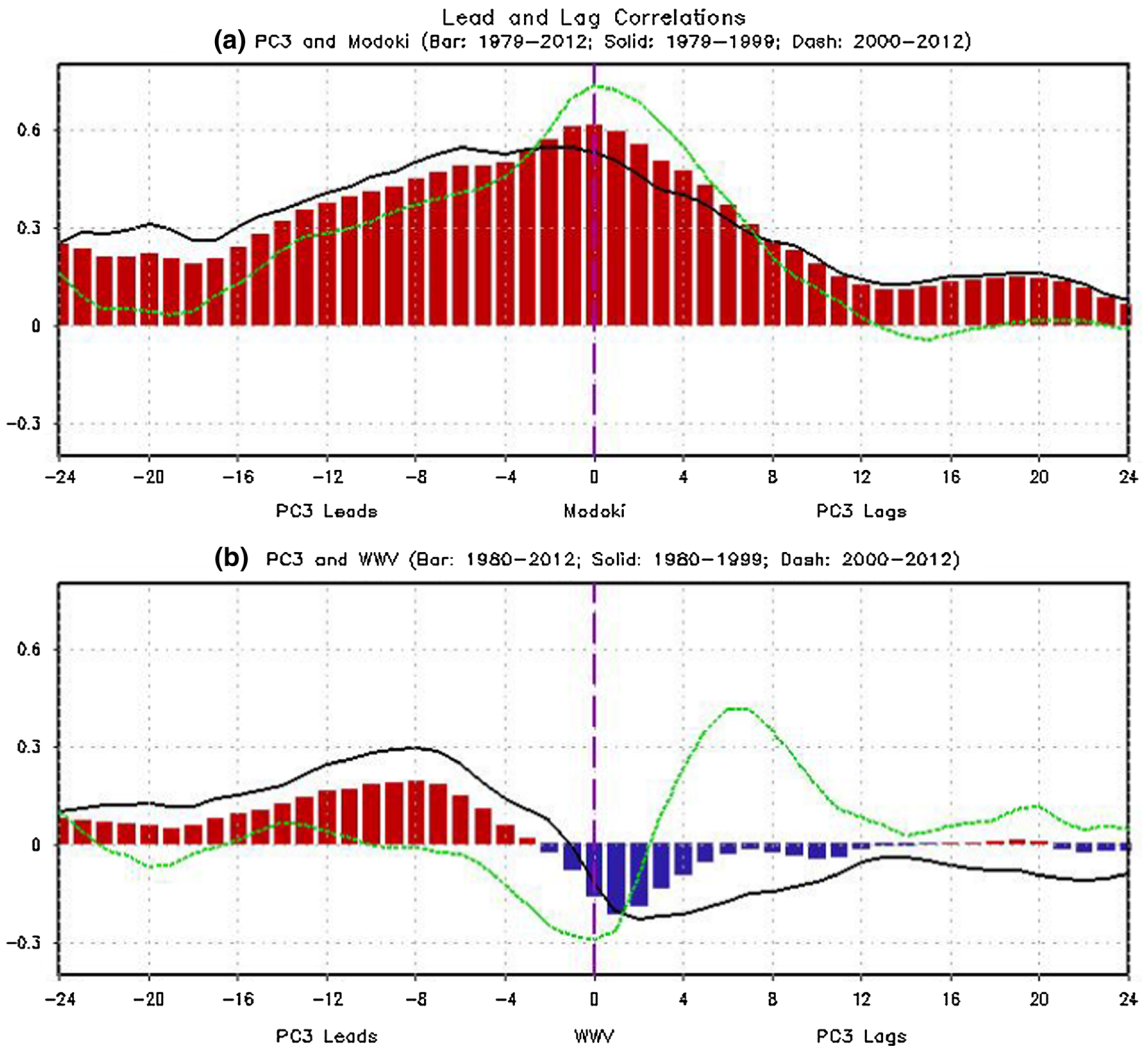

Fig. 7 Lead and lag correlations between (**a**) PC3 and ENSO Modoki index (**b**) PC3 and WWV index. *Bar* is the correlations for the whole period, *solid line* for Jan 1979/1980–Dec 1999, and *dash line* for Jan 2000–Dec 2012

based on the reconstruction of OTA associated with each mode and analyzing differences in OTA that are averaged before and after 1999/2000.

The contribution from EOF1 has a deepening (shoaling) of the thermocline in the western (eastern) Pacific (Fig. 10b, shading) and is because of the dominance of frequent La Niña events since 2000 (Fig. 1). This highlights the fact that a change in the characteristics of ENSO since 2000, with a preference for La Niña events contributed to the increase in the east–west gradient in the thermocline (McPhaden et al. 2011). Although the reconstruction based on EOF1 is consistent with the east–west pattern of the change in the thermocline, the amplitude of change in the western Pacific requires taking into account the contribution from EOF2. PC2 time-series (Fig. 4a, b) shows consistent negative values since 2000 implying a warm sub-surface temperature anomaly with maximum near the date line and to the west, and adds to the positive amplitude of change in sub-surface anomalies.

Since EOF3 has no trend, it has no significant contribution to change in the thermocline (Fig. 10c). With a sudden shift in the time-series for EOF4, this mode has a minor contribution to the change in the thermocline (Fig. 10d).

4 Summary and discussion

In this work, we analyzed the leading modes of variability of OTA along the equatorial Pacific Ocean and their connection with ENSO. Compared with corresponding modes calculated using OTA in the top 459 m for GODAS and in the top 500 m for TAO, it is noted that GODAS and TAO have almost identical patterns and similar sequence of the variances with comparable fraction explained by each one

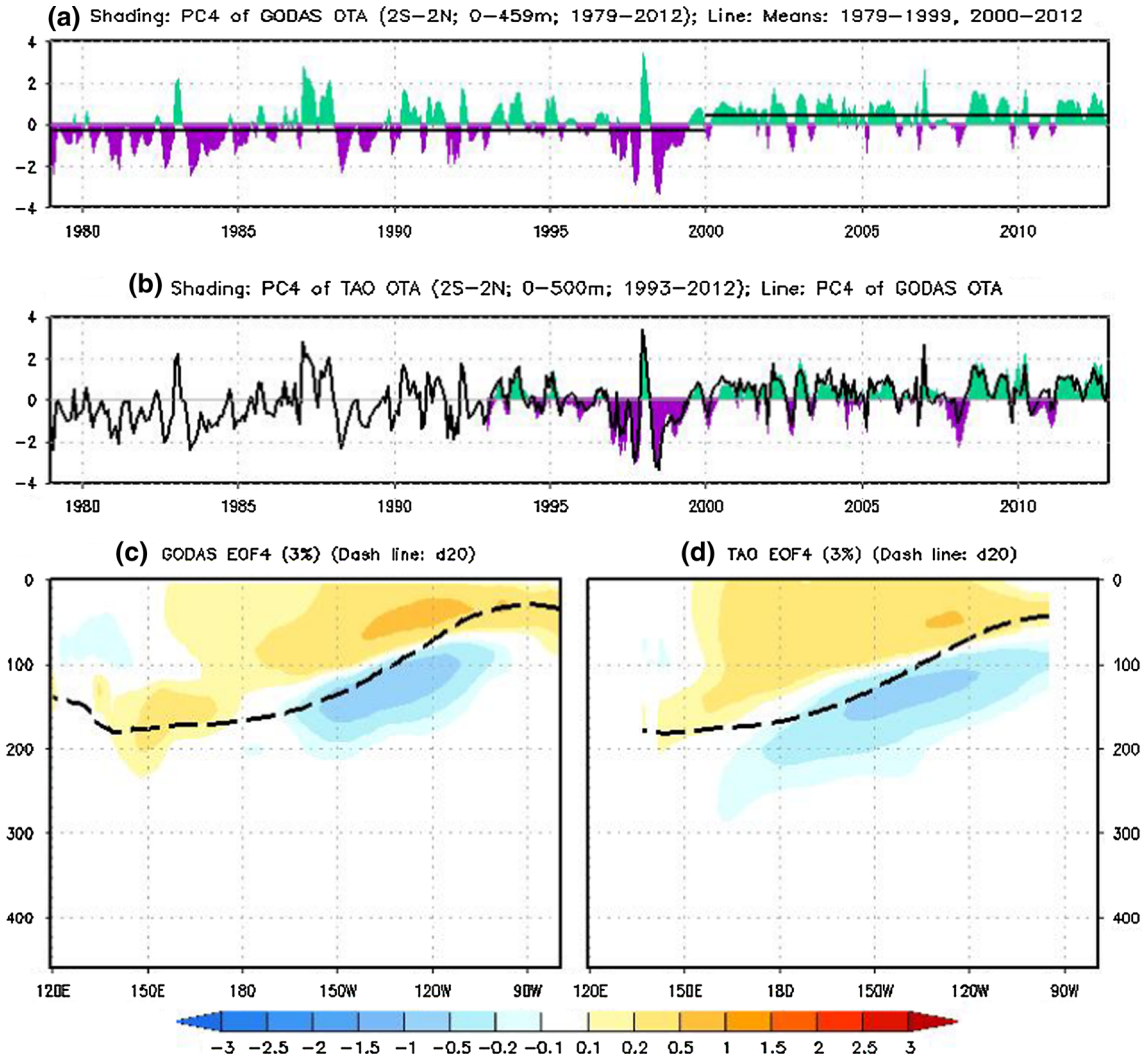

Fig. 8 Same as Fig. 1, but (**a**) PC4 of GODAS (*shading*) and the means in Jan 1979–Dec 1999 and Jan 2000–Dec 2012 (*lines*); (**b**) PC4 of TAO (*shading*) and PC4 of GODAS (*curve*); (**c**) EOF4 of GODAS; and (**d**) EOF4 of TAO. The percentage of total variance explained by this mode is 3 % for both GODAS and TAO

of the first four leading modes, suggesting the reliability of GODAS OTA data. From these modes, we note that ocean temperature variations are mainly along the thermocline between 50 and 200 m.

The first two leading modes are connected with the canonical ENSO. EOF1 is characterized by opposite variation of OTA above the thermocline in the western and along the thermocline in the eastern equatorial Pacific with magnitudes in the cold tongue larger than that in the warm pool. Spatial pattern of EOF2 shows more of a basin wide character. Based on the analysis of lead-lag correlations of PC1 and PC2 with the Niño3.4 SST index and WWV index, respectively, their connection with ENSO and WWV variability were identified. Overall, the first two modes represent the features of different phases of an ENSO cycle, as well as an asymmetric nature in its magnitude of the warm and cold phases, in its evolution with faster development and slower decay of a warm event, and in its magnitude of the associated anomalies in the western and eastern equatorial Pacific.

EOF3 shows a tripole pattern with opposite variation between OTA above the thermocline in the central Pacific and along the thermocline in the eastern and western Pacific. This mode characterizes variability associated with the so-called ENSO-Modoki. The evolution of EOF3 is weakly correlated with WWV and PC1 and PC2, suggesting that ENSO-Modoki (or the PC3) is a mode largely independent to the canonical ENSO and confirming that it is less actively involved with thermocline processes compared with that of the canonical ENSO. It has longer time scales compared with the canonical ENSO.

EOF4 represents a warming tendency above the thermocline and a cooling tendency below the thermocline since 2000. In fact, in addition to this mode, both EOF1

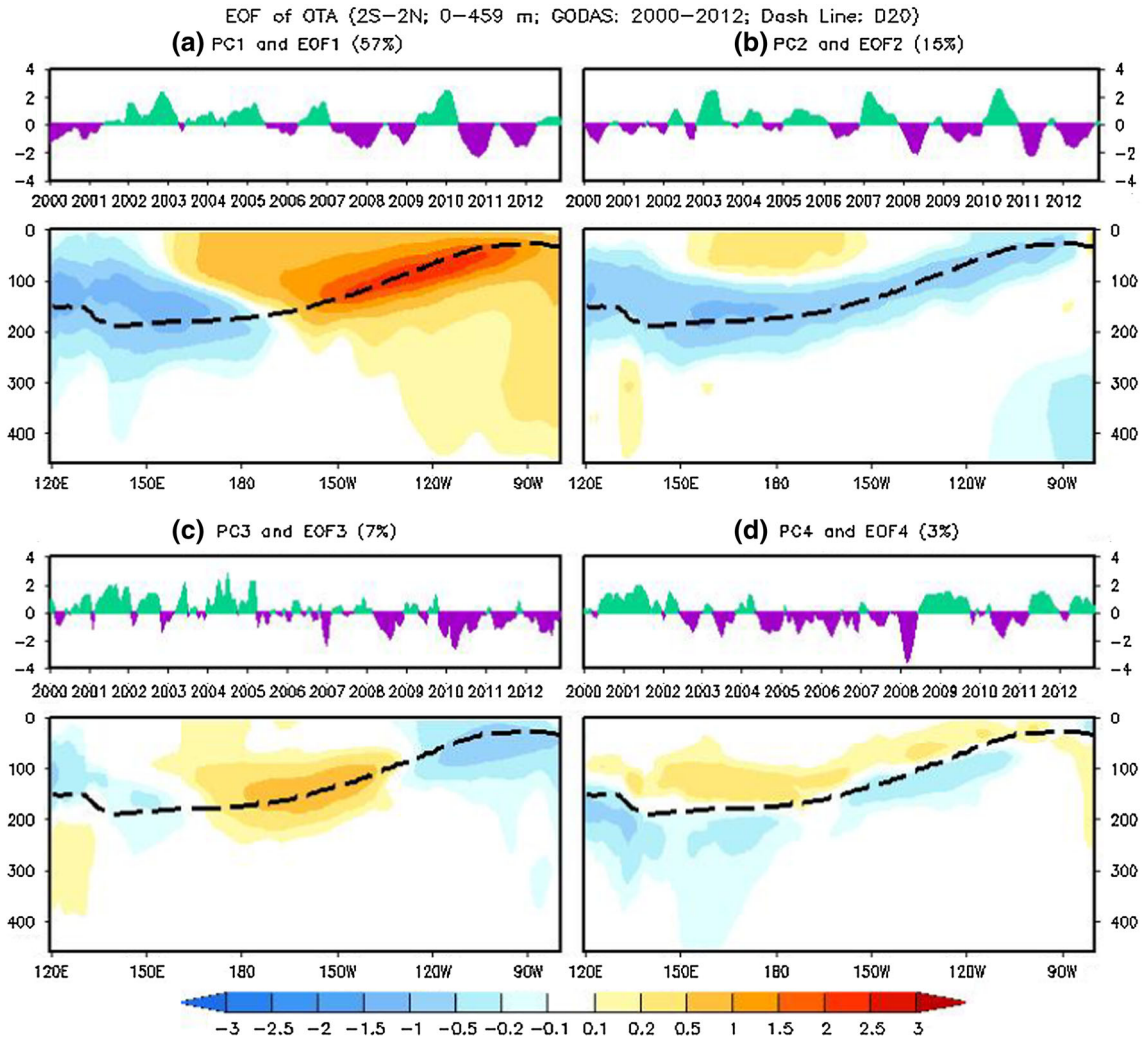

Fig. 9 First four leading EOF modes and the corresponding PCs of GODAS OTA in Jan 2000–Dec 2012. The percentages of total variance explained by these modes are 59, 15, 7, and 3 % for EOF1–4, respectively. The *dash line* is the climatological mean d20 in Jan 2000–Dec 2012

and EOF2 have even larger contributions to the change of the thermocline during 1979–2012 due to the fact of more El Niño events with large magnitudes during 1979–1999 and more frequent La Niña events since 2000. Moreover, ENSO and OTA shifted into a higher frequency regime since 2000, compared with that during 1979–1999. Interestingly, EOF3 does not have any trend or significant interdecadal shift during 1979–2012. The so-called long-term trend of ENSO-Modoki indicated in some previous works seems mainly caused by mean zonal SST gradient change (L'Heureux et al. 2013), which was used in the ENSO-Modoki definition (Ashok et al. 2007), instead of the change of this mode itself.

The analysis shows a change in characteristics of ENSO variability since 2000. This change is also accompanied with a change in the structure of the thermocline in the equatorial Pacific, and is consistent with some recent works. As documented by, such as, McPhaden (2012), Horii et al. (2012), and Hu et al. (2013a), the tropical Pacific climate system involved systematic change around 1999/2000. For example, Hu et al. (2013a) noted that compared with 1979–1999, the interannual variability in the tropical Pacific was significantly weaker in 2000–2011, and this shift can be seen by coherent changes in both the tropical atmosphere and ocean. For example, the equatorial thermocline tilt became steeper during 2000–2011, and was consistent with positive (negative) sea surface temperature anomalies, increased (decreased) precipitation, and enhanced (suppressed) convection in the western (central and eastern) tropical Pacific, which reflected an intensification of the Walker circulation. Hu et al. (2013a) further proposed that the combination of a steeper thermocline slope with stronger surface trade winds has hampered the eastward migration of the warm water along the equatorial Pacific. As a consequence, the variability of the warm water volume was reduced and thus ENSO amplitude also decreased.

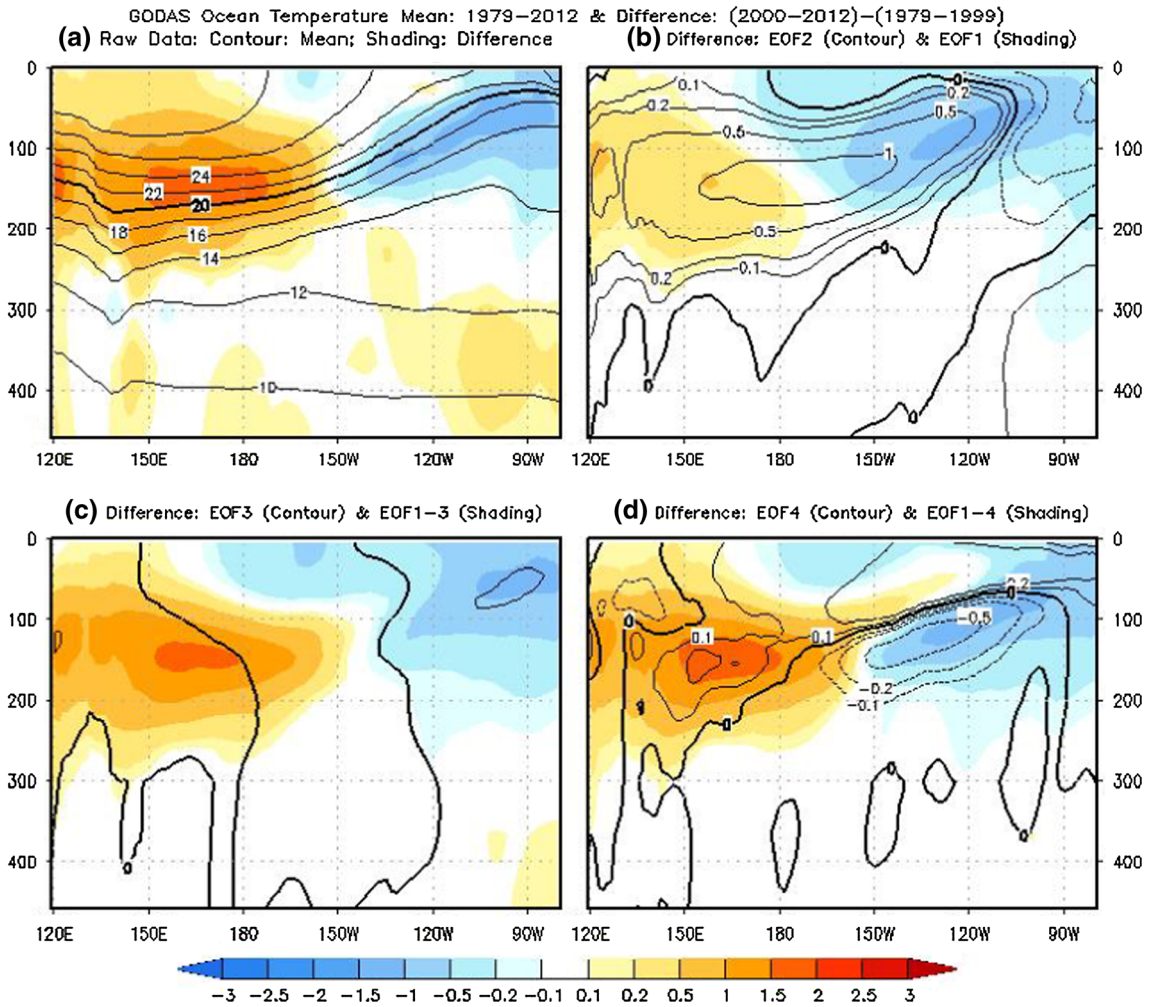

Fig. 10 (**a**) GODAS ocean temperature mean in Jan 1979–Dec 2012 (*contour*) and the difference between means in Jan 2000–Dec 2012 and in Jan 1979–Dec 1999 (*shading*). Reconstructed OTA difference based on (**b**) EOF1 (*shading*) and EOF2 (*contour*) (**c**) EOF1–3 (*shading*) and EOF3 (*contour*), and (**d**) EOF1–4 (*shading*) and EOF4 (*contour*). The contour interval is 2 °C in (**a**) and it is same as the shading interval in (**b**–**d**) indicated in the *color bar*. 20 °C *contour* in (**a**) and 0 °C *contours* in (**b**–**d**) are thickened

Several interesting questions regarding the relationship between the thermocline and ENSO can be posed, e.g., how much of the change in the thermocline is due to the change in ENSO variability (e.g., more frequent La Niña after 2000); and to what extent is the change in thermocline structure responsible for change in ENSO variability? An analysis of the modes of EOF of OTA variability allowed us to deconvolve change in the thermocline that is associated with ENSO (i.e., EOF1 of OTA), and a component that is due to increase in ocean heat content in the western Pacific/date line region related to EOF2. To what extent the latter is responsible for change in the ENSO variability remains an open question. Furthermore, it is shown that first four EOF modes are robust before and after 1999/2000, suggesting that the interdecadal shift of the climate system in the tropical Pacific is mainly a frequency shift and the spatial variation in the pattern are relatively small, although the mean states over two periods experienced some significant changes. Thus, there is another open question why the tropical Pacific coupling system shifted to higher frequency since 1999/2000.

Besides the natural variation, another potential factor causing the change in OTA and tropical Pacific mean states around 2000 in the tropical Pacific is the external forcing change: increase of greenhouse gas concentrations. For instance, in a global warming scenario, it might be expected that the tropical easterly trade winds weaken, surface ocean temperatures warm fastest near the equator and more slowly farther away, and the temperature gradients across the thermocline become steeper (Collins et al. 2010). However, some observed changes after 2000 in background conditions are opposite to those expected from greenhouse gas forcing. It is also possible that changes in OTA in the equatorial Pacific are part of natural climate

variability that has important implications for ENSO and ENSO-Modoki variability, predictability, and prediction skill. We anticipate that the framework of monitoring leading modes of OTA variability will provide a convenient way to monitor ENSO and ENSO-Modoki variability and also low-frequency trends in thermocline variability, and help us understand interactions between them.

Acknowledgments We thank the TAO Project Office of NOAA/PMEL for supplying the TAO data, and appreciate the constructive comments of two reviewers as well as Drs. Wanqiu Wang, Yan Xue, and Hui Wang.

References

An S-I, Jin F–F (2001) Collective role of thermocline and zonal advective feedbacks in the ENSO mode. J Clim 14:3421–3432

Ashok K, Behera SK, Rao SA, Weng H, Yamagata T (2007) El Niño Modoki and its possible teleconnection. J Geophys Res 112:C11007. doi:10.1029/2006JC003798

Barnett TP, Latif M, Kirk E, Roeckner E (1991) On ENSO physics. J Clim 4(5):487–515

Behringer DW, Xue Y (2004) Evaluation of the global ocean data assimilation system at NCEP: the Pacific Ocean. Preprints, eighth symposium on integrated observing and assimilation systems for atmosphere, oceans, and land surface, Seattle, WA, Amer. Meteor Soc, 2.3 [Available online at http://ams.confex.com/ams/84Annual/techprogram/paper_70720.htm]

Bjerknes J (1969) Atmospheric teleconnections from the equatorial Pacific. Mon Weather Rev 97:163–172

Burgers G, Stephenson DB (1999) The "normality" of El Niño. Geophys Res Lett 26:1027–1030

Clarke AJ, S Van Gorder, Colantuono G (2007) Wind stress curl and ENSO discharge/recharge in the equatorial Pacific. J Phys Ocean: 37(4):1077–1091

Clarke AJ (2010) Analytical theory for the quasi-steady and low-frequency equatorial ocean response to wind forcing: the 'tilt' and 'warm water volume' modes. J Phys Ocean 40(1):121–137

Collins M et al (2010) The impact of global warming on the tropical Pacific Ocean and El Niño. Nat Geosci 3:391–397. doi:10.1038/ngeo868

Dewitte B, Thual S, Yeh S-W, An S-I, Moon B-K, Giese BS (2009) Low-frequency variability of temperature in the vicinity of the equatorial Pacific thermocline in SODA: role of equatorial wave dynamics and ENSO asymmetry. J Clim 22:5783

Di Lorenzo et al (2010) Central Pacific El Niño and decadal change in the North Pacific Oscillation. Nat Geosci 3 (11). doi:10.1038/NGEO984

Glantz MH (2000) Currents of change: impacts of El Niño and La Niña on climate and society. Cambridge, UK: Cambridge University Press, 266 pp. ISBN 052178672X

Guilyardi E et al (2009) Understanding El Niño in ocean–atmosphere general circulation models: progress and challenges. Bull Am Meteor Soc 90:325–340

Hoerling MP, Kumar A (2002) Atmospheric response patterns associated with tropical forcing. J Clim 15:2184–2203

Horii T, Ueki I, Hanawa K (2012) Breakdown of ENSO predictors in the 2000s: decadal changes of recharge/discharge-SST phase relation and atmospheric intra seasonal forcing. Geophys Res Lett 39:L10707. doi:10.1029/2012GL051740

Hu Z–Z, Kumar A, Jha B, Wang W, Huang B, Huang B (2012) An analysis of warm pool and cold tongue El Niños: air-sea coupling processes, global influences, and recent trends. Clim Dyn 38(9–10):2017–2035. doi:10.1007/s00382-011-1224-9

Hu Z–Z, Kumar A, Ren H-L, Wang H, L'Heureux M, Jin F–F (2013a) Weakened interannual variability in the tropical Pacific Ocean since 2000. J Clim (in press)

Hu Z–Z, A Kumar, Y Xue, B Jha (2013b) Why were some La Niñas followed by another La Niña? Clim Dyn (submitted)

Huang B, Xue Y, Zhang D, Kumar A, McPhaden MJ (2010) The NCEP GODAS ocean analysis of the tropical Pacific mixed layer heat budget on seasonal to interannual time scales. J Clim 23(18):4901–4925

Jin F–F (1997a) An equatorial ocean recharge paradigm for ENSO. Part I: conceptual model. J Atmos Sci 54:811–829

Jin F–F (1997b) An equatorial ocean recharge paradigm for ENSO. Part II: a stripped-down coupled model. J Atmos Sci 54:830–847

Kanamitsu M et al (2002) NCEP-DOE AMIP-II reanalysis (R-2). Bull Am Meteor 83:1631–1643

Kao H-Y, Yu J-Y (2009) Contrasting eastern-Pacific and central-Pacific types of ENSO. J Clim 22:615–632

Kessler WS (2002) Is ENSO a cycle or a series of events? Geophys Res Lett 29(23):2125. doi:10.1029/2002GL015924

Kim ST, Yu J-Y, Kumar A, Wang H (2012) Central-Pacific El Niño in the NCEP CFS model and its extratropical associations. Mon Weather Rev 140:1908–1923

Kug J-S, Jin F–F, An S-I (2009) Two types of El Niño events: cold tongue El Niño and warm pool El Niño. J Clim 22:1499–1515. doi:10.1175/2008JCLI2624.1

Kug J-S, Choi J, An S-I, Jin F–F, Wittenberg AT (2010) Warm pool and cold tongue El Niño events as simulated by the GFDL 2.1 coupled GCM. J Clim 23:1226–1239

Kumar A, Zhang Q, Peng P, Jha B (2005) SST-forced atmospheric variability in an atmospheric general circulation model. J Clim 18:3953–3967

Kumar A, Chen M, Zhang L, Wang W, Xue Y, Wen W, Marx L, Huang B (2012) An analysis of the nonstationarity in the bias of sea surface temperature forecasts for the NCEP climate forecast system (CFS) version 2. Mon Weather Rev 140: 3003–3016. http://dx.doi.org/10.1175/MWR-D-11-00335.1

L'Heureux M, Collins D, Hu Z–Z (2013) Linear trends in sea surface temperature of the tropical Pacific Ocean and implications for the El Niño-Southern Oscillation. Clim Dyn 40(5–6):1223–1236. doi:10.1007/s00382-012-1331-2

McPhaden MJ (1993) TOGA-TAO and the 1991–93 El Niño Southern Oscillation event. Oceanography 6(2):36–44

McPhaden MJ (2012) A 21st century shift in the relationship between ENSO SST and warm water volume anomalies. Geophys Res Lett 39:L09706. doi:10.1029/2012GL051826

McPhaden MJ, Lee T, McClurg D (2011) El Niño and its relationship to changing background conditions in the tropical Pacific Ocean. Geophys Res Lett 38:L15709. doi:10.1029/2011GL048275

Meinen CS, McPhaden MJ (2000) Observations of warm water volume changes in the equatorial Pacific and their relationship to El Niño and La Niña. J Clim 13:3551–3559

Moon B-K et al (2004) Vertical structure variability in the equatorial Pacific before and after the Pacific climate shift of the 1970s. Geophys Res Lett 31(3):L03203. doi:10.1029/2003GL018829

National Research Council (2010) Assessment of intraseasonal to interannual climate prediction and predictability. The National Academies Press: Washington, 192 pp. ISBN-10: 0-309-15183-X

Neelin JD et al (1998) ENSO theory. J Geophys Res 103:14261–14290

Okumura YM, Deser C (2010) Asymmetry in the duration of El Niño and La Niña. J Clim 23:5826–5843

Okumura YM, Ohba M, Deser C, Ueda H (2011) A proposed mechanism for the asymmetric duration of El Niño and La Niña. J Clim 24:3822–3829. doi:10.1175/2011JCLI3999.1

Philander SGH (1990) El Niño, La Niña and the Southern Oscillation. Academic Press, San Diego, 293 pp. ISBN 0125532350

Picaut J, Ioualalen M, Menkes C, Delcroix T, McPhaden MJ (1996) Mechanism of the zonal displacements of the Pacific warm pool: implications for ENSO. Science 274:1486–1489

Ropelewski C, Halpert M (1987) Global and regional scale precipitation patterns associated with the El Niño-Southern Oscillation. Mon Weather Rev 115:1606–1626

Smith TM, Reynolds RW, Peterson TC, Lawrimore J (2008) Improvements to NOAA's historical merged land-ocean surface temperature analysis (1880–2006). J Clim 21:2283–2296

Trenberth KE, Smith L (2006) The vertical structure of temperature in the tropics: different flavors of El Niño. J Clim 19:4956–4973

Vimont DJ, Alexander M, Fontaine A (2009) Mid-latitude excitation of tropical variability in the Pacific: the role of thermodynamic coupling and seasonality. J Clim 22:518–534

Wang C, Picaut J (2004) Understanding ENSO physics—a review. Earth's climate: the ocean-atmosphere interaction. In: C Wang, S-P Xie, JA Carton (Eds.) AGU Geophys Monogr Ser, 147: 21–48

Wang W, Chen M, Kumar A (2010) An assessment of the CFS real-time seasonal forecasts. Weather Forecast 25:950–969. doi:10.1175/2010WAF2222345.1

Weare BC, Navato AR, Newell RE (1976) Empirical orthogonal analysis of Pacific sea surface temperatures. J Phys Ocean 6:671–678

Xue Y, Chen M, Kumar A, Hu Z–Z, Wang W (2013) Prediction skill and bias of tropical Pacific sea surface temperatures in the NCEP climate forecast system version 2. J Clim (in press)

Yu J-Y, Kao H-Y, Lee T, Kim ST (2011) Subsurface ocean temperature indices for Central-Pacific and Eastern-Pacific types of El Niño and La Niña events. Theor Appl Clim 103(3–4): 337–344. doi:10.1007/s00704-010-0307-6

Zhang R-H, Levitus S (1996) Structure and evolution of interannual variability of the tropical Pacific upper ocean temperature. J Geophys Res 101:20501–20524

Zhang R-H, Levitus S (1997) Interannual variability of the coupled tropical Pacific ocean-atmosphere system associated with the El Nino/Southern Oscillation. J Clim 10:1312–1330